Study of Higgs-gauge boson anomalous couplings through $e^-e^+ \rightarrow W^-W^+h$ at the ILC

Satendra Kumar,[*] P. Poulose,[†] and Shibananda Sahoo[‡]

Department of Physics, Indian Institute of Technology Guwahati, Guwahati 781 039, India
(Received 19 February 2015; published 29 April 2015)

Higgs couplings with gauge bosons are probed through $e^-e^+ \rightarrow W^-W^+h$ in an effective Lagrangian framework. An ILC of 500 GeV center-of-mass energy with possible beam polarization is considered for this purpose. The reach of the ILC with integrated luminosity of 300 fb^{-1} in the determination of both the charge conjugation and parity (CP)-conserving and CP-violating parameters is obtained. Sensitivity of the probe of each of these couplings on the presence of other couplings is investigated. The most influential coupling parameters are $\bar{c}_W = -\bar{c}_B$. Other parameters of significant effect are $\bar{c}_{HW}$ and $\bar{c}_{HB}$ among the CP-conserving ones and $\tilde{c}_{HW}$ among the CP-violating ones. CP-violating parameters $\tilde{c}_\gamma$ and $\tilde{c}_{HB}$ are found to have very little influence on the process considered. A detailed study of the angular distributions presents a way to disentangle the effect of some of these couplings.

PACS numbers: 12.15.-y, 13.66.Fg, 14.70.Fm

I. INTRODUCTION

The discovery of the new resonance of mass around 126 GeV by the ATLAS and CMS collaborations at the LHC [1–13] provides a gateway to the investigations of the dynamics of elementary particles. The discovery has unambiguously established the role of the Higgs mechanism in electroweak symmetry breaking (EWSB). All of the properties of the new particle measured so far are consistent with that of the standard Higgs boson. Thus, one may be tempted to conclude that for all practical purposes, the newly found particle is like that of the Standard Model (SM) Higgs boson, and new physics effects are decoupled as far as the Higgs sector is concerned. At the same time, it is well known that there are difficulties associated with the Higgs sector of the SM that need to be addressed. The main difficulty is the hierarchy problem associated with the quadratically diverging quantum corrections to the mass of the Higgs boson when computed in the SM. There is no remedy to this difficulty within the SM, and for a Higgs boson of mass 126 GeV, the new physics effects should show up within the TeV range to cure this malady. Assuming that the new physics effects are expected to appear only indirectly in the Higgs sector, it is natural to consider these effects through effective couplings of the Higgs bosons with itself as well as with the gauge bosons and heavy fermions. Precise measurement of these couplings is very essential to establish the true nature of the EWSB mechanism. While the LHC is capable of probing some of these couplings [14], especially the Higgs couplings with the gauge bosons and top quark, one may need to rely on a cleaner machine like the International Linear

[*]satendra@iitg.ernet.in
[†]poulose@iitg.ernet.in
[‡]shibananda@iitg.ernet.in

Collider (ILC) [15–18] for the required precision. Another aspect that is very important to investigate is the CP properties of the couplings of the Higgs boson. Although the measurements so far indicate a CP-even Higgs boson, it is not ruled out that the Higgs sector does not involve any CP violation. One may remember that one of the compelling reasons to look beyond the SM is the large CP violation necessary to understand the baryon asymmetry of the Universe. There have been many studies on the CP properties of the Higgs boson in the past [19]. More recently, there have been studies on the CP properties of the Higgs interaction with the top quark [20], investigating the influence of a CP-mixed Higgs boson on the Yukawa couplings. Within an effective Lagrangian, the effect of new physics could be studied in the various couplings through the quantum corrections they acquire. Such an effective Lagrangian basically encodes the new physics effects in higher-dimensional operators with anomalous couplings.

The study of the Higgs sector through an effective Lagrangian goes back to Refs. [21–33]. More recently, the Lagrangian including a complete set of dimension-six operators was studied by Refs. [34–37]. For some of the recent references discussing the constraints on the anomalous couplings within different approaches, please see Refs. [38–51]. Reference [49] studied the $h + V$, where $V = Z, W$, associated production at the LHC and Tevatron to discuss the bounds obtainable from the global fit to the presently available data, whereas Ref. [50] has discussed the constraint on the parameters coming from the LHC results as well as other precision data from the LEP, SLC, and Tevatron. Experimental studies on the Higgs couplings at the LHC are presented in, for example, Refs. [52,53]. The measurement of trilinear Higgs couplings is best done through the process $e^+e^- \rightarrow Zhh$ [54–64]. At the same time, this process also depends on the Higgs-gauge boson

couplings, ZZh and $ZZhh$, which will affect the determination of the hhh coupling. Another process that could probe the hhh couplings is $e^+e^- \to \nu_e\bar{\nu}_e hh$ following the WW fusion [58–61], which is also affected by the WWh and $WWhh$ couplings. In a recent study [65], we investigated the effect of the VVh coupling, where $V = Z, W$ in the extraction of the hhh coupling and found that a precise knowledge of the WWh and ZZh couplings is necessary to derive information regarding the trilinear couplings.

The process $e^+e^- \to W^-W^+h$ is well suited to study the Higgs to gauge boson couplings [54–64]. At the same time, this process also depends on the trilinear gauge boson couplings like $WW\gamma$, which can contaminate the effects of Higgs to gauge boson couplings. In this paper, we will focus our attention on this process in some detail within the framework of the effective Lagrangian. One goal of this study is to investigate CP violation in the Higgs sector through Higgs to gauge boson couplings and to understand the significance of other couplings in their measurement.

The paper is presented in the following way. In Sec. II, the effective Lagrangian will be presented, with the currently available constraint on the parameters. In Sec. III, the process under consideration will be presented with details. In Sec. IV, the results will be summarized.

II. GENERAL SETUP

References [29–32,36,49,66] present the most general effective Lagrangian with dimension-six operators involving the Higgs bosons. Part of this Lagrangian relevant to the process $e^+e^- \to W^-W^+h$ considered in this paper is given by

$$\mathcal{L}_{\text{Higgs}}^{\text{CPC}} = \frac{\bar{c}_H}{2v^2}\partial^\mu(\Phi^\dagger\Phi)\partial_\mu(\Phi^\dagger\Phi) + \frac{\bar{c}_T}{2v^2}(\Phi^\dagger\overset{\leftrightarrow}{D}{}^\mu\Phi)(\Phi^\dagger\overset{\leftrightarrow}{D}_\mu\Phi) - \frac{\bar{c}_6}{v^2}\lambda(\Phi^\dagger\Phi)^3 + \frac{\bar{c}_\gamma}{m_W^2}g'^2\Phi^\dagger\Phi B_{\mu\nu}B^{\mu\nu}$$
$$+ \frac{ig\bar{c}_{HW}}{m_W^2}(D^\mu\Phi^\dagger\sigma_k D^\nu\Phi)W_{\mu\nu}^k + \frac{ig'\bar{c}_{HB}}{m_W^2}(D^\mu\Phi^\dagger D^\nu\Phi)B_{\mu\nu} + \frac{ig\bar{c}_W}{2m_W^2}(\Phi^\dagger\sigma_k\overset{\leftrightarrow}{D}{}^\mu\Phi)D^\nu W_{\mu\nu}^k + \frac{ig'\bar{c}_B}{2m_W^2}(\Phi^\dagger\overset{\leftrightarrow}{D}{}^\mu\Phi)\partial^\nu B_{\mu\nu},$$

$$\mathcal{L}^{\text{CPV}} = \frac{ig\tilde{c}_{HW}}{m_W^2}D^\mu\Phi^\dagger T_{2k}D^\nu\Phi\tilde{W}_{\mu\nu}^k + \frac{ig'\tilde{c}_{HB}}{m_W^2}D^\mu\Phi^\dagger D^\nu\Phi\tilde{B}_{\mu\nu} + \frac{g'^2\tilde{c}_\gamma}{m_W^2}\Phi^\dagger\Phi B_{\mu\nu}\tilde{B}_{\mu\nu} + \frac{g^3\tilde{c}_{3W}}{m_W^2}\epsilon_{ijk}W_{\mu\nu}^i W_\rho^{\nu j}\tilde{W}^{\rho\mu k}, \tag{1}$$

where the dual field strength tensors are defined as $\tilde{B}_{\mu\nu} = \frac{1}{2}\epsilon_{\mu\nu\rho\sigma}B^{\rho\sigma}$, $\tilde{W}_{\mu\nu}^k = \frac{1}{2}\epsilon_{\mu\nu\rho\sigma}W^{\rho\sigma k}$, and $\Phi^\dagger\overset{\leftrightarrow}{D}_\mu\Phi = \Phi^\dagger(D_\mu\Phi) - (D_\mu\Phi^\dagger)\Phi$, with D_μ being the appropriate covariant derivative operator and Φ the usual Higgs doublet in the SM. Also, $W_{\mu\nu}^k$ and $B_{\mu\nu}$ are the field tensors corresponding to the $SU(2)_L$ and $U(1)_Y$ of the SM gauge groups, respectively, with gauge couplings g and g', in that order. σ_k are the Pauli matrices, and λ is the usual (SM) quadratic coupling constant of the Higgs field. The above Lagrangian leads to the following CP-conserving ($\mathcal{L}_{hV}^{\text{CPC}}$) and CP-violating ($\mathcal{L}_{hV}^{\text{CPV}}$) parts in the unitary gauge and mass basis [66]:

$$\mathcal{L}_{hV}^{\text{CPC}} = -\frac{1}{4}g_{hzz}^{(1)}Z_{\mu\nu}Z^{\mu\nu}h - g_{hzz}^{(2)}Z_\nu\partial_\mu Z^{\mu\nu}h + \frac{1}{2}g_{hzz}^{(3)}Z_\mu Z^\mu h - \frac{1}{2}g_{h\gamma z}^{(1)}Z_{\mu\nu}F^{\mu\nu}h$$
$$- g_{h\gamma z}^{(2)}Z_\nu\partial_\mu F^{\mu\nu}h - \frac{1}{8}g_{hhzz}^{(1)}Z_{\mu\nu}Z^{\mu\nu}h^2 - \frac{1}{2}g_{hhzz}^{(2)}Z_\nu\partial_\mu Z^{\mu\nu}h^2 + \frac{1}{4}g_{hhzz}^{(3)}Z_\mu Z^\mu h^2$$
$$- \frac{1}{2}g_{hww}^{(1)}W^{\mu\nu}W_{\mu\nu}^\dagger h - [g_{hww}^{(2)}W^\nu\partial^\mu W_{\mu\nu}^\dagger h + \text{H.c.}] + gm_W W_\mu^\dagger W^\mu h$$
$$- \frac{1}{4}g_{hhww}^{(1)}W^{\mu\nu}W_{\mu\nu}^\dagger h^2 - \frac{1}{2}[g_{hhww}^{(2)}W^\nu\partial^\mu W_{\mu\nu}^\dagger h^2 + \text{H.c.}] + \frac{1}{4}g^2 W_\mu^\dagger W^\mu h^2, \tag{2}$$

$$\mathcal{L}_{3V} = [ig_{\gamma ww}^{(1)}W_{\mu\nu}^\dagger A^\mu W^\nu + \text{H.c.}] + ig_{\gamma ww}^{(2)}F_{\mu\nu}W^\mu W^{\nu\dagger} + [ig_{zww}^{(1)}W_{\mu\nu}^\dagger Z^\mu W^\nu + \text{H.c.}] + ig_{zww}^{(2)}Z_{\mu\nu}W^\mu W^{\nu\dagger}, \tag{3}$$

$$\mathcal{L}_{hV}^{\text{CPV}} = -\frac{1}{4}\tilde{g}_{h\gamma\gamma}F_{\mu\nu}\tilde{F}^{\mu\nu}h - \frac{1}{4}\tilde{g}_{hzz}Z_{\mu\nu}\tilde{Z}^{\mu\nu}h - \frac{1}{2}\tilde{g}_{h\gamma z}Z_{\mu\nu}\tilde{F}^{\mu\nu}h - \frac{1}{2}\tilde{g}_{hww}W^{\mu\nu}\tilde{W}_{\mu\nu}^\dagger h$$
$$- \frac{1}{8}\tilde{g}_{hh\gamma\gamma}F_{\mu\nu}\tilde{F}^{\mu\nu}h^2 - \frac{1}{8}\tilde{g}_{hhzz}Z_{\mu\nu}\tilde{Z}^{\mu\nu}h^2 - \frac{1}{8}\tilde{g}_{hh\gamma z}Z_{\mu\nu}\tilde{F}^{\mu\nu}h^2$$
$$- \frac{1}{4}\tilde{g}_{hhww}W^{\mu\nu}\tilde{W}_{\mu\nu}^\dagger h^2 + i\tilde{g}_{hzww}^{(1)}\tilde{Z}^{\mu\nu}W_\mu W_\nu^\dagger h - [i\tilde{g}_{hzww}^{(2)}\tilde{W}^{\mu\nu}Z_\mu W_\nu^\dagger h + \text{H.c.}]. \tag{4}$$

The physical couplings relevant to the process $e^+e^- \to WWh$ and associated with the Lagrangian in Eqs. (2)–(4) expressed in terms of the effective couplings presented in Eq. (1) are listed in Table I. In total, there are nine parameters which are relevant to the process considered, viz., $\bar{c}_T, \bar{c}_\gamma, \bar{c}_B, \bar{c}_W, \bar{c}_{HB}, \bar{c}_{HW}, \tilde{c}_{HW}, \tilde{c}_{HB}, \tilde{c}_\gamma$. Out of these, six parameters are related to CP-conserving couplings, and the other three are connected with CP-violating couplings.

TABLE I. Physical couplings in Eqs. (2)–(4) are given in terms of the effective couplings in Eq. (1), where $c_W = \cos\theta_W$ and $s_W = \sin\theta_W$, with θ_W being the weak mixing angle.

CP-conserving couplings

$$g_{hzz}^{(1)} = \frac{2g}{c_W^2 m_W}[\bar{c}_{HB}s_W^2 - 4\bar{c}_\gamma s_W^4 + c_W^2\bar{c}_{HW}]$$

$$g_{hzz}^{(2)} = \frac{g}{c_W^2 m_W}[(\bar{c}_{HW} + \bar{c}_W)c_W^2 + (\bar{c}_B + \bar{c}_{HB})s_W^2] \qquad g_{hzz}^{(3)} = \frac{gm_Z}{c_W}[1 - 2\bar{c}_T]$$

$$g_{hz\gamma}^{(1)} = \frac{gs_W}{c_W m_W}[\bar{c}_{HW} - \bar{c}_{HB} + 8\bar{c}_\gamma s_W^2] \qquad g_{hz\gamma}^{(2)} = \frac{gs_W}{c_W m_W}[\bar{c}_{HW} - \bar{c}_{HB} - \bar{c}_B + \bar{c}_W]$$

$$g_{hww}^{(1)} = \frac{2g}{m_W}\bar{c}_{HW} \qquad g_{hww}^{(2)} = \frac{g}{2m_W}[\bar{c}_W + \bar{c}_{HW}]$$

$$g_{\gamma ww}^{(1)} = e[1 - 2\bar{c}_W] \qquad g_{\gamma ww}^{(2)} = e[1 - 2\bar{c}_W - \bar{c}_{HB} - \bar{c}_{HW}]$$

$$g_{zww}^{(1)} = \frac{g}{c_W}[c_W^2 - \bar{c}_{HW} + (2s_W^2 - 3)\bar{c}_W]$$

$$g_{zww}^{(2)} = \frac{g}{c_W}[c_W^2(1 - \bar{c}_{HW}) + s_W^2\bar{c}_{HB} + (2s_W^2 - 3)\bar{c}_W]$$

CP-violating couplings

$$\tilde{g}_{h\gamma\gamma} = -\frac{8g\bar{c}_\gamma s_W^2}{m_W} \qquad \tilde{g}_{hz\gamma} = \frac{gs_W}{c_W m_W}[\tilde{c}_{HW} - \tilde{c}_{HB} + 8\tilde{c}_\gamma s_W^2]$$

$$\tilde{g}_{hzz} = \frac{2g}{c_W^2 m_W}[\tilde{c}_{HW}s_W^2 - 4\tilde{c}_\gamma s_W^4 + c_W^2\tilde{c}_{HW}] \qquad \tilde{g}_{hww} = \frac{2g}{m_W}\tilde{c}_{HW}$$

$$\tilde{g}_{hzww}^{(1)} = \frac{g^2}{c_W m_W}[\tilde{c}_{HW}(2 - s_W^2) + \tilde{c}_{HB}s_W^2] \qquad \tilde{g}_{hzww}^{(2)} = \frac{2g^2}{m_W}c_W\tilde{c}_{HW}$$

These anomalous coefficients $\bar{c}_T, \bar{c}_{HW}, \bar{c}_{HB}, \bar{c}_\gamma$ are expected to be of the order

$$\bar{c}_T \sim \mathcal{O}\left(\frac{g_{NP}^2 v^2}{M^2}\right) \quad \text{and} \quad \bar{c}_{HW}, \bar{c}_{HB}, \bar{c}_\gamma \sim \mathcal{O}\left(\frac{g_{NP}^2 M_W^2}{16\pi^2 M^2}\right), \tag{5}$$

where g_{NP} denotes the generic coupling of the new physics, and M is the new physics scale. This indicates that these couplings can be significantly large for strongly coupled physics. In contrast, the coefficients of the operators such as $\bar{c}_W$ and $\bar{c}_B$ are given by

$$\bar{c}_B, \bar{c}_W \sim \mathcal{O}\left(\frac{m_W^2}{M^2}\right) \tag{6}$$

and, therefore, expected to be relatively suppressed or enhanced according to the ratio g/g_{NP}. Coming to the experimental bounds, electroweak precision data put the following constraints [34]:

$$\bar{c}_T(m_Z) \in [-1.5, 2.2] \times 10^{-3} \quad \text{and}$$

$$(\bar{c}_W(m_Z) + \bar{c}_B(m_Z)) \in [-1.4, 1.9] \times 10^{-3}. \tag{7}$$

This means we can safely ignore the effect of $\bar{c}_T$ in our analysis. On the other hand, $\bar{c}_W$ and $\bar{c}_B$ are not independently constrained, leaving the possibility of having large values with a cancellation between them as per the above constraint. $\bar{c}_W$ itself along with $\bar{c}_{HW}$ and $\bar{c}_{HB}$ are constrained from LHC observations on the associated production of the Higgs along with W in Ref. [49]. Considering

the Higgs-associated production along with W, ATLAS and CMS along with D0 put a limit of $\bar{c}_W \in [-0.03, 0.01]$ when all other parameters were set to zero. A global fit using various information from ATLAS and CMS including signal-strength information constrains the region in the $\bar{c}_W - \bar{c}_{HW}$ plane, leading to a slightly more relaxed limit on $\bar{c}_W$ and a limit of about $\bar{c}_{HW} \in [-0.1, 0.06]$. The limit on $\bar{c}_{HB}$ estimated using a global fit in Ref. [49] is about $\bar{c}_{HB} \in [-0.05, 0.05]$ with a one-parameter fit. The *CP*-violating couplings are largely unconstrained so far.

The purpose of this study is to understand how to exploit a precision machine like the ILC to investigate a suitable process so as to derive information regarding these couplings. In the next section, we shall explain the process of interest in the present case and discuss the details to understand the influence of one or more of the couplings mentioned above.

III. ANALYSES OF THE PROCESS CONSIDERED

The Feynman diagrams corresponding to the process $e^-e^+ \to W^-W^+h$ in the SM are given in Fig. 1. This process is basically influenced by Higgs to charged gauge bosons as well as neutral gauge boson couplings like $WWh, ZZh, WW\gamma$, and WWZ, apart from the fermionic couplings, which are taken to be the standard couplings in our study.

The effective Lagrangian, Eq. (1), apart from allowing the existing Higgs and gauge boson couplings to be nonstandard, introduces new couplings which are absent in the SM. In a specific model, such effects appear at higher orders with a new particle present in the loops.
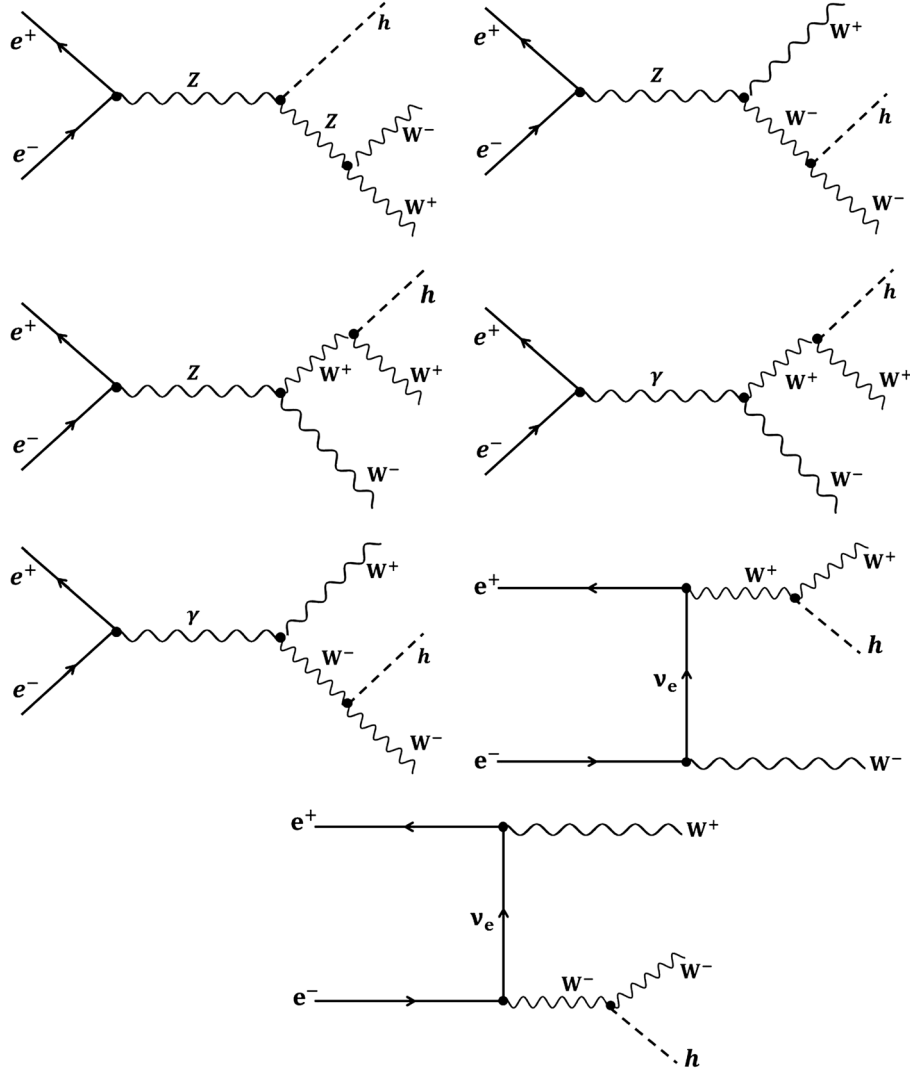
FIG. 1.   Feynman diagrams contributing to the process $e^- e^+ \rightarrow W^- W^+ h$ in the SM.

When the masses of such particles are taken to be large, the effect of such quantum correction can be considered in terms of changed couplings. Such effective couplings arising in the present analysis are presented in Table I. Our numerical analyses are carried out using MADGRAPH [67,68], with the effective Lagrangian implemented through FEYNRULES [66,69].

As the first observable, we consider the cross section. Figure 2 (left) presents the total cross section against the center-of-mass energy for the WWh production. The cross section peaks around the center-of-mass energy of 500 GeV, and, therefore, our further detailed analysis will be done for a collider of this energy. As expected, the polarization hugely improves the situation. The case of a typical polarization combination expected at the ILC, 80% left-polarized electron beam and 30% right-polarized positron beam, is considered [17], along with the case of an 80% left-polarized electron beam and a 60% right-polarized positron beam, which are expected in the upgraded version of the ILC.

In Fig. 2 (right) the cross section against an anomalous couplings parameter ($\bar{c}_W$) at fixed center-of-mass energy of 500 GeV is considered along with the role of the polarized beams. In order to be consistent with the experimental constraint [Eq. (7)], we choose $\bar{c}_B = -\bar{c}_W$ throughout our analysis. Notice that the cross section is enhanced rapidly, even for the very small values of $\bar{c}_W$, showing the high sensitivity of the cross section on this parameter. Assuming that no other couplings affect the process, the single parameter reach corresponding to the 3σ limit with 300 fb^{-1} integrated luminosity is obtained as $-0.003 \leq (\bar{c}_W = -\bar{c}_B) \leq +0.003$ in the case of unpolarized beam, which is improved to $-0.002 \leq (\bar{c}_W = -\bar{c}_B) \leq +0.002$ with an 80% left-polarized electron beam and 30% right-polarized positron beam. While the case with an 80% left-polarized electron beam and 60% right-polarized positron beam does not change this limit significantly, the cross section is increased from about 11 fb to about 14 fb, enhancing the statistics. In our further analysis, we consider
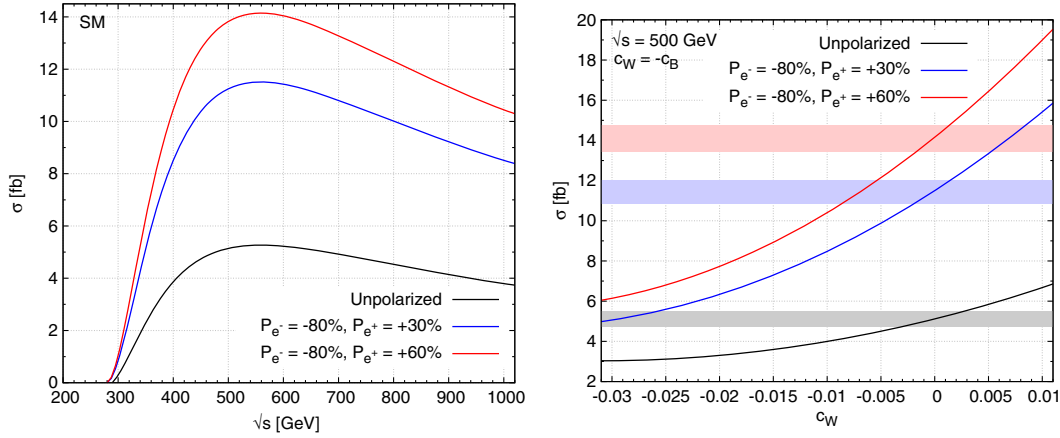
FIG. 2 (color online). Left: The total cross section against $\sqrt{s}$ in the SM. Right: The total cross section against anomalous coupling parameter ($\bar{c}_W$) at $\sqrt{s} = 500$ GeV, where the gray, blue, and red bands correspond to 3σ deviations from the SM with unpolarized and polarized beams, respectively. Note that here, as well as in all figures henceforth, we have removed the "bar" from the symbols denoting the CP-conserving parameters for convenience.

the baseline expectation of an 80% left-polarized electron beam and 30% right-polarized positron beam.

Coming to the CP-violating couplings $\tilde{c}_{HW}$, $\tilde{c}_{HB}$, and $\tilde{c}_\gamma$, the single parameter reach of the ILC at 500 GeV with 300 fb^{-1} at the 3σ level could be obtained from Figs. 3, 4, and 5, respectively. The effects of other couplings in deriving these limits are also indicated in these figures. Clearly, precise knowledge of the CP-conserving parameters $\bar{c}_W$, $\bar{c}_{HW}$, and $\bar{c}_{HB}$ is required to obtain a reasonably robust estimate of the CP-violating parameters. Among the CP-violating couplings, $\tilde{c}_{HW}$ affects the cross section most significantly, and the limits derivable on the other parameters are sensitive to their presence. The effect of the $\tilde{c}_\gamma$ is much smaller than the other couplings in finding the sensitivity of $\tilde{c}_{HW}$ and, therefore, not presented.

The correlation between the $\bar{c}_{HW}$ and $\bar{c}_{HB}$ is presented in Fig. 6, where the yellow and gray bands show the present

limits derived from the LHC results on the associated production of the Higgs boson with the W boson [49]. In the absence of any other parameter, the allowed region in the $\bar{c}_{HW} - \bar{c}_{HB}$ plane is restricted to a narrow ellipse (red). This ellipse is not affected much by the presence of $\bar{c}_W$ if it is positive (green ellipse). On the other hand, if $\bar{c}_W$ is negative, within the present bounds, it can significantly affect the allowed region (blue ellipse) in the $\bar{c}_{HW} - \bar{c}_{HB}$ plane. The presence of CP-violating parameters is found to be insignificant here.

It is essential to know the behavior of various kinematic distributions and how the anomalous coupling parameters influence these in order to derive any useful and reliable information from the experimental results. This is so, even in cases where the fitting to obtain the reach of the parameters is done with the total number of events, as the reconstruction of events and the reduction of the
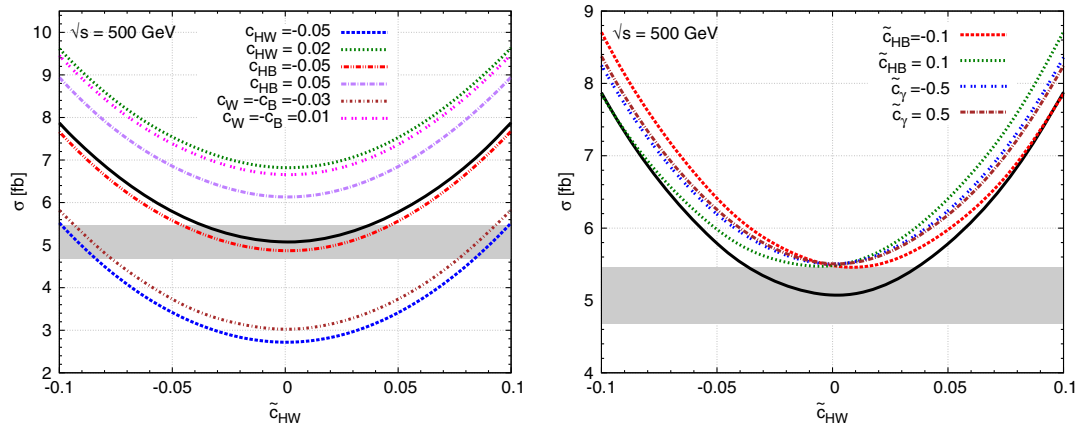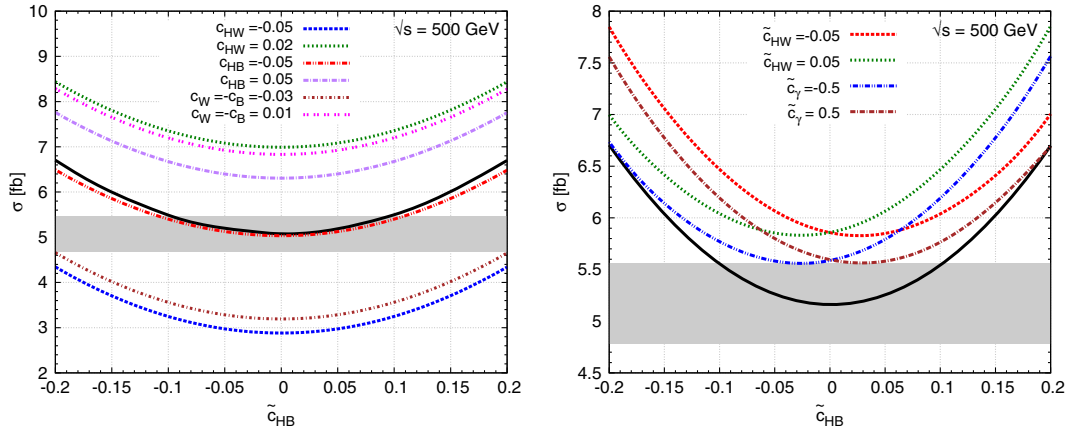

FIG. 3 (color online). Cross section against $\tilde{c}_{HW}$ in the presence of selected CP-conserving (left) and CP-violating (right) couplings. The black solid line corresponds to the case when only $\tilde{c}_{HW}$ is present. The center-of-mass energy is assumed to be $\sqrt{s} = 500$ GeV. In each case, all other parameters are set to zero. The gray band indicates the 3σ limit of the SM cross section, with an integrated luminosity of 300 fb^{-1}.

FIG. 4 (color online).   Cross section against $\tilde{c}_{HB}$ in the presence of selected *CP*-conserving (left) and *CP*-violating (right) couplings. The black solid line corresponds to the case when only $\tilde{c}_{HB}$ is present. The center-of-mass energy is assumed to be $\sqrt{s} = 500$ GeV. In each case, all other parameters are set to zero. The gray band indicates the 3σ limit of the SM cross section, with an integrated luminosity of 300 fb^{-1}.
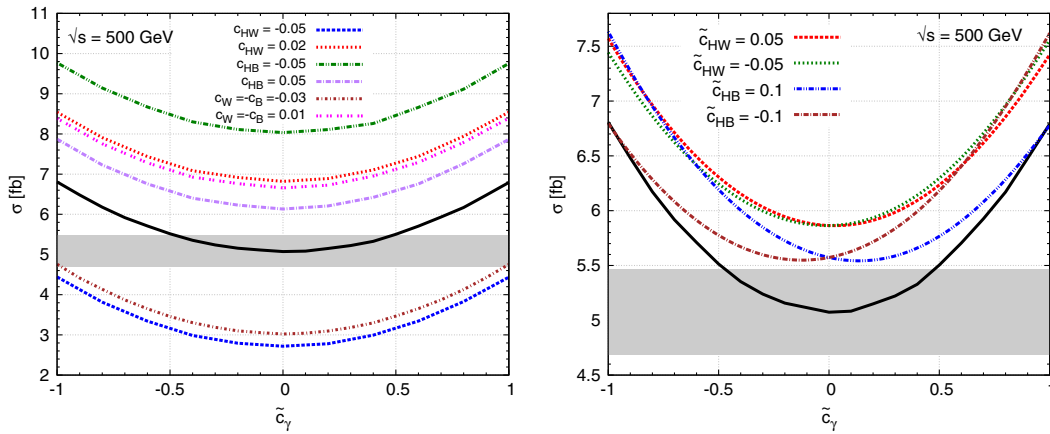

FIG. 5 (color online).   Cross section against $\tilde{c}_\gamma$ in the presence of selected *CP*-conserving (left) and *CP*-violating (right) couplings. The black solid line corresponds to the case when only $\tilde{c}_\gamma$ is present. The center-of-mass energy is assumed to be $\sqrt{s} = 500$ GeV. In each case, all other parameters are set to zero. The gray band indicates the 3σ limit of the SM cross section, with an integrated luminosity of 300 fb^{-1}.

background depend crucially on the kinematic distributions of the decay products. In the following, we shall present some illustrative cases of distributions at the production level to understand the effect of different couplings on these. The dominant decay channel for h in the signal process is $h \to b\bar{b}$, with about a 57% branching fraction. The pure hadronic (with four jets) or semileptonic (2 jets + lepton + missing energy) decay of the W pair allow one to reconstruct the events. Thus, with the final state as $WWb\bar{b}$, the $t\bar{t}$ and WWZ production processes could act as the background. The total cross section of $t\bar{t}$ and WWZ (with $Z \to b\bar{b}$) production processes are about 500 fb and about 6 fb, respectively. Both of these processes could be contained with the help of the invariant mass distribution of the $b\bar{b}$ pair ($M_{b\bar{b}}$). In the case of a signal process, this is expected to peak at the Higgs mass of about

125 GeV, while in the case of the WWZ process, it is expected to peak around the Z mass of about 91 GeV. Thus, the WWZ background could be taken care of without much trouble. On the other hand, in the case of $t\bar{t}$ pair production, the $M_{b\bar{b}}$ distribution is spread out. As presented in Fig. 7, in the relevant window of 124–128 GeV of the $M_{b\bar{b}}$, we have about 900 signal events and 2700 background events at 300 fb^{-1} integrated luminosity, leading to a large signal significance of about 15. Of course, this estimate is considering an ideal setting, whereas the reconstruction efficiencies, detector effect, etc., would bring this down considerably. However, one may expect a large significance even after these realistic considerations. Presently, we would like to be content with the analysis at the production level, considering the limited scope of this work. As mentioned earlier, we shall focus on an ILC running at a
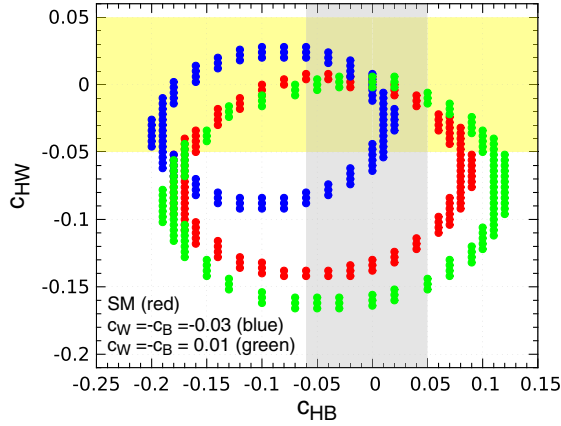
FIG. 6 (color online). The ellipses correspond to regions in the $\bar{c}_{HB} - \bar{c}_{HW}$ plane with the total cross section within the 3σ limit of the SM cross section (red), and cross sections with $\bar{c}_W = -0.03$ (blue) and $\bar{c}_W = +0.01$ (green). An integrated luminosity of 300 fb^{-1} is considered, and the center-of-mass energy is taken as 500 GeV. The yellow and gray bands correspond to the present limits of $\bar{c}_{HW}$ and $\bar{c}_{HB}$, respectively.
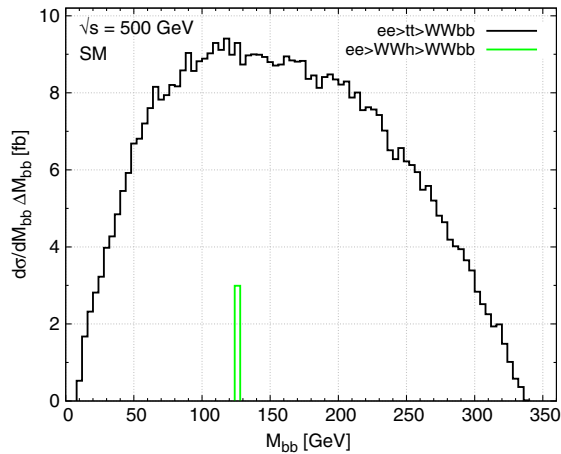

FIG. 7 (color online). Invariant mass of $b\bar{b}$ in the signal (green) and background $t\bar{t}$ (black) processes at a center-of-mass energy of $\sqrt{s} = 500$ GeV with unpolarized beams in the Standard Model case.

center-of-mass energy of 500 GeV for our study. In order to understand the interplay of CP-conserving and CP-violating couplings, we consider $\bar{c}_W$ and $\bar{c}_{HW}$ only with the CP-violating couplings.

The effect of the anomalous couplings on the kinematic distributions are presented in Figs. 8–11. The couplings $\tilde{c}_{HB}$ and $\tilde{c}_\gamma$ are found to have no significant effect, with or without the presence of other parameters and, therefore, are not presented here. In the figures, the couplings other than those mentioned are set to zero. The parameters having a significant effect are the CP-violating couplings $\tilde{c}_{HW}$ and the CP-conserving couplings $\bar{c}_W$ and $\bar{c}_{HW}$. The parameter choices considered for these numerical analyses are

$$\bar{c}_W = -0.03, +0.01, \qquad \bar{c}_{HW} = -0.05, +0.02,$$

$$\tilde{c}_{HW} = 0.1.$$

While for $\bar{c}_W$, the maximum allowed values as per the present bounds are used, in the case $\bar{c}_{HW}$, it is somewhat arbitrary but within the limits. In the case of the CP-violating parameter $\tilde{c}_{HW}$, no such limits exist, and we have considered a conservative choice of an arbitrary value to illustrate its influence. Unlike the case of $\bar{c}_W$ [as seen in Fig. 2 (right)], the sign of $\tilde{c}_{HW}$ is irrelevant, as seen in the symmetric plots in Fig. 3. While considering beam polarization, an 80% left-polarized electron beam and a 30% right-polarized positron beam are assumed, as is expected in the first phase of the ILC according to the present baseline design.

We first consider in Fig. 8 the normalized $\cos\theta_h$ distributions of the Higgs boson for the SM case, as well as different cases with anomalous couplings (both CP conserving and violating) as indicated in the figure, while all other parameters are set to zero. The normalized distributions provide clear information on the shape of the distribution, bringing out the qualitative difference between the different cases considered. The shape of the distribution remains more or less the same as that of the SM case, except a small enhancement in the central regions when both the couplings are nonzero (green curves). The advantage of beam polarization is evident (figure on the right) when compared to the corresponding unpolarized (figure on the left) case. Here, the case of negative $\bar{c}_W$ differs from the other cases. This feature can be exploited to discriminate this case from others.

Figure 9 (left) presents the normalized $\cos\theta_{W^+}$ distribution (unpolarized beams). The negative value of $\bar{c}_W$ changes the nature of the distribution drastically (dashed magenta) compared to the SM case (solid black), while all other cases have insignificant deviation. This again can be a useful discriminator of the case, but unlike the case of $\cos\theta_h$ distribution, visible deviation is present even in the presence of nonzero $\tilde{c}_{HW}$. The presence of beam polarization leaves the shape of the distribution largely unchanged. At the same time, as seen earlier, the cross section itself is enhanced by a factor of a little more than 2. Figure 9 (right) shows the normalized $\cos\theta_{W^+h}$ distribution (unpolarized beams), where θ_{W^+h} is the angle between h and W^+. Here, $\tilde{c}_{HW}$ has significant effect, which is not affected by the presence of $\bar{c}_W$. Thus, an enhancement in the backward region and a corresponding decrease in the forward region compared to the SM case indicate nonzero $\tilde{c}_{HW}$. On the other hand, the presence of negative $\bar{c}_W$ (dashed magenta) alone has the opposite effect. This along with $\cos\theta_{W^+h}$ will be able to fix the case between the presence of $\tilde{c}_{HW}$, $\bar{c}_W$ alone or together. Here again, it is seen that the use of polarized beams, while helping improve the statistics, keeps the qualitative features unchanged. Considering these three angular distributions together might allow us to
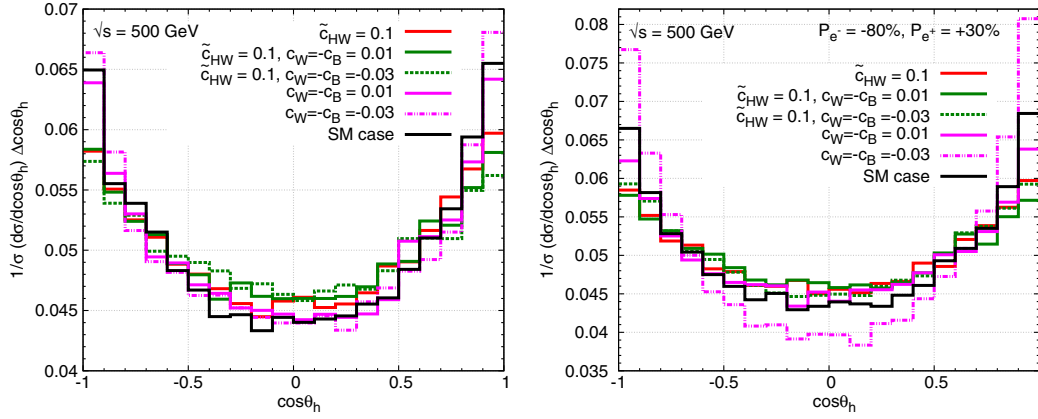
FIG. 8 (color online). Distribution of $\cos\theta_h$ for different anomalous couplings with unpolarized (left) and polarized with $P_{e^-} = -80\%, P_{e^+} = +30\%$ (right) beams. A center-of-mass energy of 500 GeV is assumed.
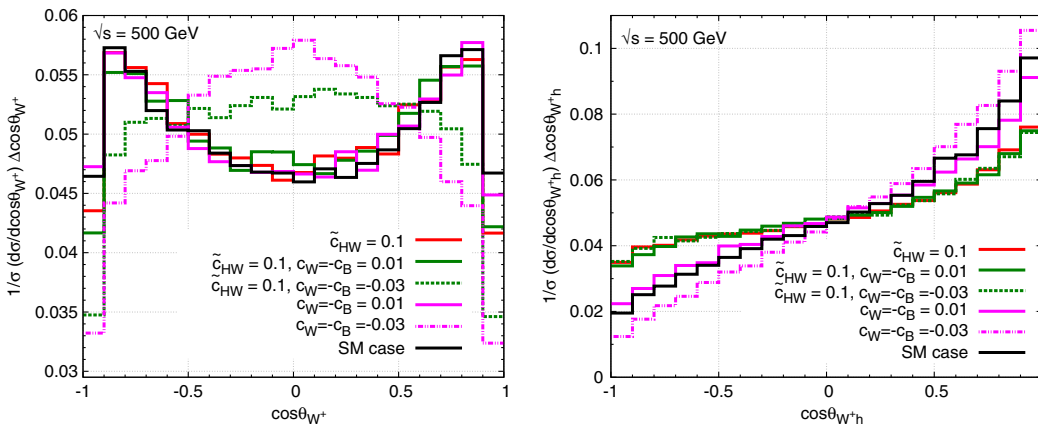

FIG. 9 (color online). Distribution of $\cos\theta_{W^+}$ (left) and $\cos\theta_{W^+h}$ (right) for different anomalous couplings with unpolarized beams. A center-of-mass energy of 500 GeV is assumed.
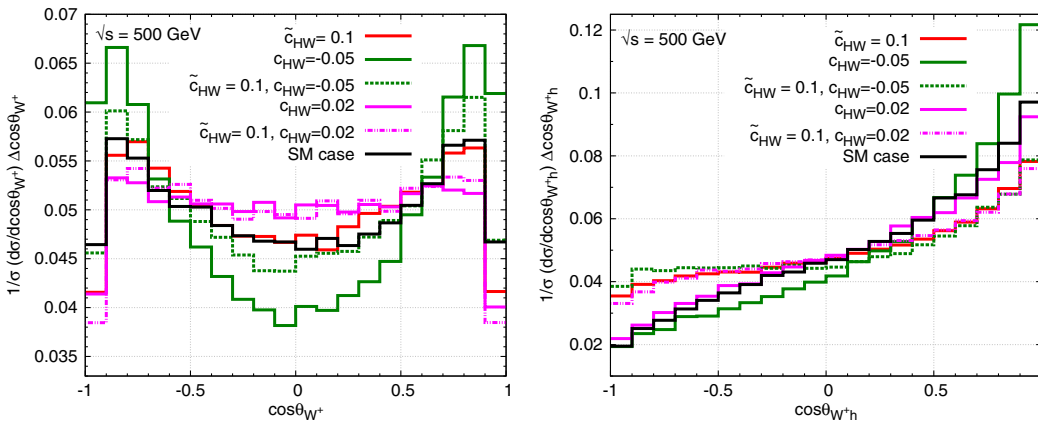

FIG. 10 (color online). Distribution of $\cos\theta_{W^+}$ (left) and $\cos\theta_{W^+h}$ (right) for different anomalous coupling values. A center-of-mass energy of 500 GeV is assumed. The color coding is the same in both figures.

distinguish different scenarios. For example, if $\tilde{c}_{HW}$ alone is present, we may expect a significant effect in the $\cos\theta_h$ and $\cos\theta_{W^+h}$ distributions, whereas the $\cos\theta_{W^+}$ distribution remains more or less unaffected. Along with $\tilde{c}_{HW}$, if $\bar{c}_W$

was present (either positive or negative), the effect in $\cos\theta_h$ is nullified, whereas the effect would remain in $\cos\theta_{W^+h}$. The change in $\cos\theta_{W^+}$ as shown in Fig. 9 (left) indicates the presence of the negative value of $\bar{c}_W$ with or without the
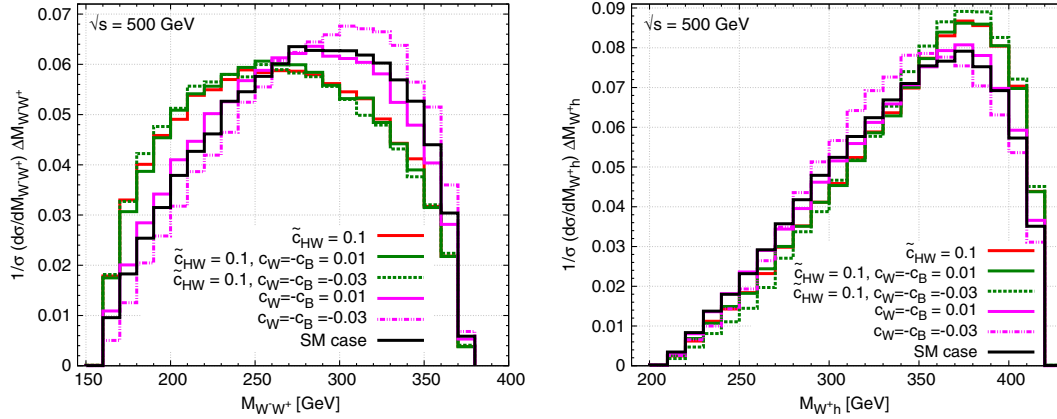
FIG. 11 (color online). The invariant mass distribution of W^-W^+ (left) and W^+h (right) for different anomalous coupling values. A center-of-mass energy of 500 GeV is assumed. The color coding is the same as in Fig. 8.

presence of other couplings. Table II summarizes the cases that could be distinguished.

Figure 9 suggests that the forward-backward asymmetry is a quantitative estimator of the presence of anomalous couplings. The percentage of deviation from the SM case for the cases of a considered set of parameters at fixed center-of-mass energy of 500 GeV without and with polarized beams is given in Table III, where the asymmetry is defined as

$$A_{\mathrm{FB}} = \frac{[\int_{-1}^{0} \frac{d\sigma}{d\cos\theta} d\cos\theta - \int_{0}^{1} \frac{d\sigma}{d\cos\theta} d\cos\theta]}{[\int_{-1}^{0} \frac{d\sigma}{d\cos\theta} d\cos\theta + \int_{0}^{1} \frac{d\sigma}{d\cos\theta} d\cos\theta]}, \quad (8)$$

TABLE II. Presence (yes) or absence (no) of deviations that could be expected in case of different scenarios with combinations of $\bar{c}_W$ and $\tilde{c}_{HW}$ realized from Figs. 8 and 9.

Couplings	$\cos\theta_h$	$\cos\theta_{W^+}$	$\cos\theta_{W^+h}$
$\tilde{c}_{HW}$ alone	Yes	No	Yes
$\bar{c}_W$ (positive) alone	No	No	No
$\bar{c}_W$ (negative) alone	Yes	Yes	Yes
$\tilde{c}_{HW}$ and $\bar{c}_W$ (positive)	No	No	Yes
$\tilde{c}_{HW}$ and $\bar{c}_W$ (negative)	No	Yes	Yes

TABLE III. Observed forward-backward asymmetry and its deviation from the SM in the angular distribution ($\cos\theta_{W^+h}$) at center-of-mass energy of 500 GeV.

$\tilde{c}_{HW}$	$\bar{c}_W = -\bar{c}_B$	$\Delta A_{\mathrm{FB}}(\cos\theta_{W^+h})\%$	
		Unpolarized beams	$P_{e^-} = -80\%$, $P_{e^+} = 30\%$
0.1	0	50	53
0.1	0.01	52	52
0.1	−0.03	52	63
0	0.01	13	11
0	−0.03	31	43
SM case;		0.3117	0.3102
$A_{\mathrm{FB}} =$			

$$\Delta A_{\mathrm{FB}}(\%) = \frac{|A_{\mathrm{FB}}^{\mathrm{ano}} - A_{\mathrm{FB}}^{\mathrm{SM}}|}{A_{\mathrm{FB}}^{\mathrm{SM}}} \times 100. \quad (9)$$

The case of $\bar{c}_{HW}$ along with CP-violating parameters also presents a similar picture. In Fig. 10, we present $\cos\theta_{W^+}$ and $\cos\theta_{W^+h}$ as an example ($\bar{c}_{HB}$ is found to be less sensitive). Here again the influence of $\bar{c}_{HW}$ on the sensitivity of $\tilde{c}_{HW}$ is clear. Similar features are also present in other kinematic distributions like $\cos\theta_h$ and $\cos\theta_{W^+}$. Unlike the case of $\bar{c}_W$ (presented in Figs. 8 and 9), here we do not find possibilities to distinguish different scenarios with the help of these distributions.

Finally, we consider the normalized invariant mass distributions of W^-W^+ and W^+h. Figure 11 presents the sensitivity of invariant mass distribution to the anomalous coupling parameters for the same set of parameters as in the inset of Fig. 8. The combinations of the parameters affected are similar to the case of $\cos\theta_{W^+h}$. This can, thus, provide an additional tool to distinguish these scenarios.

Note that in all cases, the beam polarization is found to be useful in terms of improved sensitivity with more than double the number of events compared to the case of the unpolarized beam, while keeping the qualitative features (shape of the curve) unaffected (except in the case of $\cos\theta_h$ distributions, where the shape is different in the case of $\bar{c}_W = -0.03$). Thus, the reach of the probe of the couplings can be improved by a factor of 1.5 to 2 in all cases.

IV. SUMMARY AND CONCLUSIONS

The discovery of the Higgs boson by the ATLAS and CMS collaborations at the LHC has confirmed the Higgs mechanism as the way to have EWSB providing masses to the fundamental particles. The properties of the Higgs boson measured by the LHC so far are consistent with the expectations of the SM. It is expected that the LHC would measure the mass, spin, and parity of this particle along with the standard decay widths somewhat precisely. On the other hand, details of the couplings like the trilinear and

quartic self-couplings as well as the couplings with the gauge bosons are not expected to be measured precisely. At the same time, precise knowledge of these couplings is very important in reconstructing the EWSB mechanism. A precision machine like the ILC is expected to help in the precise measurement of these couplings. In this paper, the process $e^-e^+ \rightarrow W^-W^+h$, which is influenced by the Higgs to gauge boson couplings, namely, WWh, $WW\gamma$, and ZZh, is considered. The reach of an ILC at $\sqrt{s} = 500$ GeV with an integrated luminosity of 300 fb^{-1} in probing the different relevant parameters of the corresponding effective Lagrangian is presented. The influence of the presence of other couplings in the probe of each of the couplings is studied. In general, it is observed that the CP-violating coupling $\tilde{c}_\gamma$ has very small effect on almost all of the observables considered. Study of the $\bar{c}_{HW} - \bar{c}_{HB}$ plane shows that the allowed region can be narrowed to a very small band. While this band is unaffected by the presence of $\bar{c}_W > 0$, the effect is significant if $\bar{c}_W < 0$. Consideration of the angular distributions of the Higgs boson ($\cos\theta_h$), the W boson ($\cos\theta_{W^+}$), and the distributions of the angle between W^+ and h, ($\cos\theta_{W^+h}$) proves to provide a handle in distinguishing the presence of different combinations of $\bar{c}_W$ and $\tilde{c}_{HW}$. All other parameters have an indistinguishable effect on these distributions. The invariant mass distributions of the W^-W^+ pair as well as the W^+h pair are also sensitive to some combinations of the above parameters. A quantitative estimate of the forward-backward asymmetry corresponding to the angle between W^+ and h shows that large deviations of up to 50% are possible for moderate values of the couplings. In all cases, a suitably chosen beam polarization is found to be advantageous, as illustrated with an 80% left-polarized electron beam and 30% right-polarized positron beam. The statistics can be improved by a factor of 2 with the baseline polarization quoted above, which can be improved to an enhancement factor of 3 with the expected 60% positron beam polarization in the upgraded version of the ILC. This, along with the fact that the qualitative features of the distributions in almost all cases are kept more or less intact, can be used to improve the reach of the ILC in probing these couplings significantly (almost a factor of 2). In at least one case of $\cos\theta_h$ distribution, we notice a qualitative change in the case of nonzero $\bar{c}_W$ when all other couplings are absent. Apart from the overall normalizing factor, some details are also affected, as is illustrated in the improvements in the forward-backward asymmetry, when beam polarization is used. Thus, the study shows that WWh production at the ILC is useful in detecting the anomalous couplings in Higgs-gauge boson interactions. A detailed analysis involving standard kinematic distributions could be used to distinguish different scenarios involving the couplings. While the numerical study needs to be improved with more realistic collider and detector information, as well as study of the background processes, we hope to have conveyed the importance of the process in determining and disentangling the effects of anomalous Higgs-gauge boson couplings.

---

[1] S. Chatrchyan *et al.* (CMS Collaboration), Phys. Lett. B **716**, 30 (2012).

[2] ATLAS Collaboration, Phys. Lett. B **716**, 1 (2012).

[3] ATLAS Collaboration, Report No. ATLAS-CONF-2013-029, 2013, http://cds.cern.ch/record/1527124/files/ATLAS-CONF-2013-029.pdf.

[4] ATLAS Collaboration, Report No. ATLAS-CONF-2013-013, 2013, http://cds.cern.ch/record/1523699/files/ATLAS-CONF-2013-013.pdf.

[5] ATLAS Collaboration, Report No. ATLAS-CONF-2013-031, 2013, http://cds.cern.ch/record/1527127/files/ATLAS-CONF-2013-031.pdf.

[6] CMS Collaboration, Report No. HIG-13-002-pas, 2013, http://cds.cern.ch/record/1523767/files/HIG-13-002-pas.pdf.

[7] CMS Collaboration, Report No. HIG-13-003-pas, 2013, http://cds.cern.ch/record/1523673/files/HIG-13-003-pas.pdf.

[8] G. Aad *et al.* (ATLAS Collaboration), Phys. Lett. B **726**, 88 (2013).

[9] S. Chatrchyan *et al.* (CMS Collaboration), Phys. Lett. B **716**, 30 (2012).

[10] S. Chatrchyan *et al.* (CMS Collaboration), J. High Energy Phys. 06 (2013) 081.

[11] G. Aad *et al.* (ATLAS Collaboration), Phys. Lett. B **716**, 1 (2012).

[12] V. Khachatryan *et al.* (CMS Collaboration), Eur. Phys. J. C **74**, 3076 (2014).

[13] G. Aad *et al.* (ATLAS Collaboration), Phys. Rev. D **90**, 112015 (2014).

[14] E. Gabrielli, M. Heikinheimo, L. Marzola, B. Mele, C. Spethmann, and H. Veermae, Phys. Rev. D **89**, 053012 (2014).

[15] J. Brau *et al.* (ILC Collaboration), arXiv:0712.1950.

[16] G. Aarons *et al.* (ILC Collaboration), arXiv:0709.1893.

[17] G. Moortgat-Pick, T. Abe, G. Alexander, B. Ananthanarayan, A. A. Babich, V. Bharadwaj, D. Barber, A. Bartl *et al.*, Phys. Rep. **460**, 131 (2008).

[18] E. Boos, V. Bunichev, M. Dubinin, and Y. Kurihara, Phys. Lett. B **739**, 410 (2014).

[19] A. Freitas and P. Schwaller, Phys. Rev. D **87**, 055014 (2013).

[20] B. Ananthanarayan, S. K. Garg, C. S. Kim, J. Lahiri, and P. Poulose, Phys. Rev. D **90**, 014016 (2014).

[21] S. Weinberg, Physica (Amsterdam) **96A**, 327 (1979).

[22] S. Weinberg, Phys. Lett. **91B**, 51 (1980).

[23] H. Georgi, Annu. Rev. Nucl. Part. Sci. **43**, 209 (1993).

[24] W. Buchmuller and D. Wyler, Nucl. Phys. **B268**, 621 (1986).

[25] K. Hagiwara, S. Ishihara, R. Szalapski, and D. Zeppenfeld, Phys. Rev. D **48**, 2182 (1993).

[26] K. Hagiwara, R. Szalapski, and D. Zeppenfeld, Phys. Lett. B **318**, 155 (1993).

[27] S. Alam, S. Dawson, and R. Szalapski, Phys. Rev. D **57**, 1577 (1998).

[28] V. Barger, T. Han, P. Langacker, B. McElrath, and P. Zerwas, Phys. Rev. D **67**, 115001 (2003).

[29] G. F. Giudice, C. Grojean, A. Pomarol, and R. Rattazzi, J. High Energy Phys. 06 (2007) 045.

[30] R. Contino, C. Grojean, M. Moretti, F. Piccinini, and R. Rattazzi, J. High Energy Phys. 05 (2010) 089.

[31] R. Contino, arXiv:1005.4269.

[32] R. Grober and M. Muhlleitner, J. High Energy Phys. 06 (2011) 020.

[33] B. Grzadkowski, M. Iskrzynski, M. Misiak, and J. Rosiek, J. High Energy Phys. 10 (2010) 085.

[34] M. Baak, M. Goebel, J. Haller, A. Hoecker, D. Kennedy, R. Kogler, K. Mönig, M. Schott, and J. Stelzer, Eur. Phys. J. C **72**, 2205 (2012).

[35] M. B. Einhorn and J. Wudka, Nucl. Phys. **B876**, 556 (2013).

[36] R. Contino, M. Ghezzi, C. Grojean, M. Muhlleitner, and M. Spira, J. High Energy Phys. 07 (2013) 035.

[37] S. Willenbrock and C. Zhang, Annu. Rev. Nucl. Part. Sci. **64**, 83 (2014).

[38] F. Bonnet, M. B. Gavela, T. Ota, and W. Winter, Phys. Rev. D **85**, 035016 (2012).

[39] T. Corbett, O. J. P. Eboli, J. Gonzalez-Fraile, and M. C. Gonzalez-Garcia, Phys. Rev. D **86**, 075013 (2012).

[40] W. F. Chang, W. P. Pan, and F. Xu, Phys. Rev. D **88**, 033004 (2013).

[41] J. Elias-Miro, J. R. Espinosa, E. Masso, and A. Pomarol, J. High Energy Phys. 11 (2013) 066.

[42] S. Banerjee, S. Mukhopadhyay, and B. Mukhopadhyaya, Phys. Rev. D **89**, 053010 (2014).

[43] E. Boos, V. Bunichev, M. Dubinin, and Y. Kurihara, Phys. Rev. D **89**, 035001 (2014).

[44] E. Masso and V. Sanz, Phys. Rev. D **87**, 033001 (2013).

[45] Z. Han and W. Skiba, Phys. Rev. D **71**, 075009 (2005).

[46] T. Corbett, O. J. P. Eboli, J. Gonzalez-Fraile, and M. C. Gonzalez-Garcia, Phys. Rev. D **87**, 015022 (2013).

[47] B. Dumont, S. Fichet, and G. von Gersdorff, J. High Energy Phys. 07 (2013) 065.

[48] A. Pomarol and F. Riva, J. High Energy Phys. 01 (2014) 151.

[49] J. Ellis, V. Sanz, and T. You, J. High Energy Phys. 07 (2014) 036.

[50] H. Belusca-Maito, arXiv:1404.5343.

[51] R. S. Gupta, A. Pomarol, and F. Riva, Phys. Rev. D **91**, 035001 (2015).

[52] ATLAS Collaboration, Phys. Lett. B **726**, 88 (2013).

[53] D. Teyssier (ATLAS and CMS Collaborations), arXiv: 1404.7311.

[54] A. De Rujula, M. B. Gavela, P. Hernandez, and E. Masso, Nucl. Phys. **B384**, 3 (1992).

[55] A. Gutierrez-Rodriguez, M. A. Hernandez-Ruiz, O. A. Sampayo, A. Chubykalo, and A. Espinoza-Garrido, J. Phys. Soc. Jpn. **77**, 094101 (2008).

[56] Y. Takubo, arXiv:0907.0524.

[57] J. Tian, K. Fujii, and Y. Gao, arXiv:1008.0921.

[58] M. Battaglia, E. Boos, and W. M. Yao, Studying the Higgs Potential at the e + e− Linear Collider, eConf 010630, E3016 (2001).

[59] V. Barger, T. Han, P. Langacker, B. McElrath, and P. Zerwas, Phys. Rev. D **67**, 115001 (2003).

[60] R. Killick, K. Kumar, and H. E. Logan, Phys. Rev. D **88**, 033015 (2013).

[61] A. Djouadi, W. Kilian, M. Muhlleitner, and P. M. Zerwas, Eur. Phys. J. C **10**, 27 (1999).

[62] H. Baer, T. Barklow, K. Fujii, Y. Gao, A. Hoang, S. Kanemura, J. List, H. E. Logan et al., arXiv:1306.6352.

[63] C. Castanier, P. Gay, P. Lutz, and J. Orloff, in 2nd ECFA/ DESY Study 1998–2001, pp. 1362–1372.

[64] K. Fujii, in *Proceedings of the Higgs Snowmass Workshop, Princeton, New Jersey, 2013* [slides available from http:// physics.princeton.edu/indico/conferenceDisplay.py?confId =127].

[65] S. Kumar and P. Poulose, arXiv:1408.3563.

[66] A. Alloul, B. Fuks, and V. Sanz, J. High Energy Phys. 04 (2014) 110.

[67] J. Alwall, M. Herquet, F. Maltoni, O. Mattelaer, and T. Stelzer, J. High Energy Phys. 06 (2011) 128.

[68] J. Alwall, R. Frederix, S. Frixione, V. Hirschi, F. Maltoni, O. Mattelaer, H.-S. Shao, T. Stelzer, P. Torrielli, and M. Zaro, J. High Energy Phys. 07 (2014) 079.

[69] FeynRules, http://feynrules.irmp.ucl.ac.be/wiki/HEL.